JAMSTEC Rep. Res. Dev., Volume 22, March 2016, 1–12
doi: 10.5918/jamstecr.22.1

—Original Paper—

Beam Blockage Identification for Weather Radars on board the R/V *Mirai* Using Archived Data

Biao Geng[1*] and Masaki Katsumata[1]

The Doppler weather radar on board the research vessel *Mirai*, which was installed in 1998, was replaced by a dual-polarization Doppler weather radar in 2014. This study explores the beam blockage for both radars on board the *Mirai*. Reflectivity data from long-term observations were used to calculate the probability of detection (POD) at a given range, azimuth, and elevation relative to the *Mirai*. Azimuthal sectors suffering from beam blockage caused by the infrastructure of the *Mirai* were characterized by pronounced minima of the POD in their centers and significant discontinuities of the POD on their edges. An objective method was developed to ascertain the boundaries of the blocked sectors based on the rate of change of the POD gradient along the azimuthal direction. According to the distinct signatures of the POD, detailed beam blockage information for both radars was identified in different ship-relative elevations. Although beam blockage for both radars occurred from low to high elevations, the total azimuths of the low-level blocked sectors for the dual-polarization Doppler radar decreased by more than half. This improvement was attributed to the higher location of the antenna for the dual-polarization Doppler radar. This accurate beam blockage information will facilitate the quality control of the *Mirai* radar data.

Keywords : R/V *Mirai*, shipboard weather radar, beam blockage

Received 29 September 2015 ; Revised 3 December 2015 ; Accepted 3 December 2015

1 Research and Development (R&D) Center for Global Change (RCGC), Japan Agency for Marine-Earth Science and Technology (JAMSTEC)

*Corresponding author:
Biao Geng
Research and Development (R&D) Center for Global Change, Japan Agency for Marine-Earth Science and Technology
2-15 Natsushima-cho, Yokosuka, Kanagawa 237-0061, Japan
bgeng@jamstec.go.jp

1. Introduction

Precipitation has a substantial effect on global climate change, and weather radar is one of the most powerful tools for observing various precipitation systems. Observational data from weather radar facilitate the study of precipitation systems and the quantitative estimation of rainfall, which play important roles in climate systems.

A Doppler weather radar was installed on board the research vessel *Mirai* in 1998 (Yoneyama, 1998). Since then, the Doppler radar has been used to observe precipitation systems over open oceans. By using the observational data of the Doppler radar on board the *Mirai*, characteristics of precipitation systems have been studied in the tropical Pacific Ocean (Katsumata and Yoneyama, 2004; Geng et al., 2011), the tropical Indian Ocean (Yamada et al., 2010; Yoneyama et al., 2013), and the Arctic Ocean (Inoue et al., 2010). In 2014, the Doppler radar was replaced by a dual-polarization Doppler weather radar (hereafter referred to as dual-polarization radar) (Katsumata, 2014). The dual-polarization radar began to be used for the observation of oceanic precipitation systems from the boreal summer of 2014.

Radar data quality control is important because quantitative precipitation estimation is often based on radar data. One of the major factors affecting radar data quality is beam blockage (Joss and Waldvogel, 1990). Beam blockage occurs when radar beams are partially or totally blocked by nearby obstacles. On land, beam blockage is typically caused by terrain and buildings. Because the *Mirai* is used for observations over open oceans, terrain and buildings are not present. As will be shown in detail in section 2, however, the infrastructure of the *Mirai* induces severe blockage in some radar sectors. The radar signals may be significantly degraded or completely lost if the beams are partially or totally obscured, thus inducing severely biased reflectivity and precipitation estimates (Vivekanandan et al., 1999; Young et al., 1999; Westrick et al., 1999; Villarini and Krajewski, 2010). The quality of dual-polarization measurements is also affected by beam blockage (Giangrande and Ryzhkov, 2005; Lang et al., 2009). As a result, radar data quality control must correct or remove the data affected by beam blockage.

The identification of regions where beam blockage occurs is a fundamental requirement for radar data quality control. There are two major approaches currently in use to identify beam blockage and develop a beam blockage elevation map for a radar system.

The first approach is based on digital terrain data and a radio propagation model (Bech et al., 2003; Kucera et al., 2004; Bech et al., 2007). This approach assesses blocked rays by calculating interactions between radar beams and digital terrain maps. Several studies have applied this technique to the identification of beam blockage (Krajewski et al., 2006; Shakti et al., 2013). It has been noted that man-made objects surrounding radar systems can scarcely be derived from the digital terrain data. This is particularly true for the ship infrastructure surrounding the *Mirai* radars. In fact, detailed three-dimensional coordinates of the ship infrastructure relative to the *Mirai* radars are unavailable now. Consequently, this method would not be effective in identifying beam blockage for the *Mirai* radars.

The second approach is based on a statistical analysis of reflectivity data from long-term measurements. This approach accumulates reflectivity data on rainy days at a fixed azimuth, elevation, and range. Beam blockage is then detected by looking for azimuth patterns of significantly weak echoes. This method utilizes reflectivity climatology around a radar system. Reflectivity climatology has been applied to both the identification of beam blockage (Sugier et al., 2002; Chang et al., 2009; Lakshmanan et al., 2012) and the validation of the first approach (Kucera et al., 2004; Krajewski et al., 2006). The *Mirai* Doppler radar has logged a great number of observations on precipitation systems since 1998. In addition, the new *Mirai* dual-polarization radar has also observed a substantial number of precipitation systems in its first half-year of service. Thus, it appears that reflectivity climatology could be a suitable technique for investigating beam blockage in the *Mirai* radars.

Few studies have examined the blocking of radar beams by the infrastructure of the *Mirai*. One exception is the study by Katsumata et al. (2008), who analyzed the reflectivity data collected by the Doppler radar on board the *Mirai* during the MISMO (Mirai Indian Ocean cruise for the Study of the MJO-convection Onset) period (Yoneyama et al., 2008a). They subjectively flagged azimuths as suffering from beam blockage if their mean reflectivity was more than 3 dB lower than that in the surrounding areas. There are no studies, however, that have comprehensively investigated the blocking of radar beams for both the Doppler and dual-polarization radars on board the *Mirai*. This study sought to fill this gap by developing an objective method

to explore beam blockage for the *Mirai* radars through the application of reflectivity climatology, which has been proven to facilitate the identification of beam blockage for ground-based radars (e.g., Sugier et al., 2002; Chang et al., 2009; Lakshmanan et al., 2012).

This paper is organized as follows. Section 2 provides an overview on features of the *Mirai* radars and their observed blocked reflectivity. Detailed processes for using archived reflectivity data to identify beam blockage are presented in section 3. The characteristics of beam blockage for the *Mirai* radars are described in section 4. Section 5 discusses the potential applications of this study, and a summary and conclusions are presented in section 6.

2. Overview of the *Mirai* radars and blocked reflectivity

The major features of the Doppler and dual-polarization radars on board the *Mirai* are listed in Table 1. Compared to the Doppler radar, there were two major changes in the dual-polarization radar. First, the magnetron transmitter was replaced by a solid-state transmitter. In addition, the diameter of the antenna was increased by 1 m and the installation height of the antenna rose by 3 m.

The antenna of the dual-polarization radar was installed at the same location as the Doppler radar. Figure 1 shows photographs illustrating the infrastructure and the radomes on board the *Mirai*. As indicated in the figure, the antennas were surrounded by ship infrastructure. The facilities of the marine-radar mast and masts for restricted maneuvering light on the bow side may block radar beams. Furthermore, radar beams may also be blocked by the aft mast, funnel, and satellite downlink antenna infrastructure on the stem side.

Two examples of the reflectivity observed by the Doppler radar at an elevation of 0.5 degrees are shown in Fig. 2. The heading direction of the *Mirai* is shown by an open arrow at the center of each example. Both examples show that rainfall occurred in a wide area around the radar. However, there were six azimuthal sectors (indicated by filled arrows) where echoes were missing or significantly deficient from the radar. Three of these sectors were on the bow side, and three others were on the stern side of the radar.

Figure 3 shows two examples of the horizontal distribution of the reflectivity measured by the dual-polarization radar. Among a large area of precipitation, there were also two azimuthal sectors with missing or significantly deficient echoes from the radar. One sector was on the bow side, and the other was on the stern side of the radar.

The appearance of sectors with missing data or significantly decreased reflectivity from the radars demonstrates the total or partial beam blockage caused by the infrastructure of the *Mirai* (Fig. 1). The *Mirai* typically keeps moving when it is deployed for research observations. Because beam blockage is caused by the infrastructure of the *Mirai*, it is clear from Figs. 2 and 3 that the azimuthal directions of the blocked sectors vary in a similar way to the change in the heading of the ship.

Table 1. Basic characteristics of the Doppler and dual-polarization radars.

	Doppler radar	Dual-polarization radar
Transmitter	Magnetron	Solid state
Frequency	5290 MHz	5370 MHz
Beam width	< 1.4 degrees	< 1.0 degrees
Antenna diameter	3 meters	4 meters
Antenna height	21 meters above sea level	24 meters above sea level
Polarization	Horizontal polarization	Simultaneous horizontal and vertical polarizations

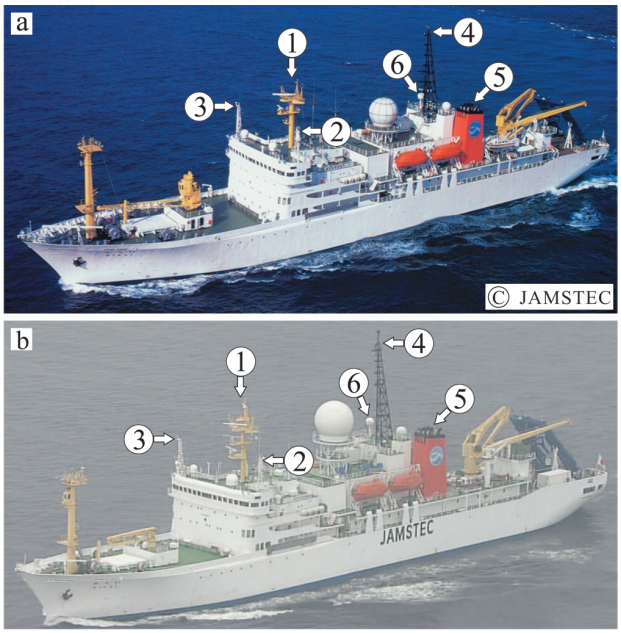

Fig. 1. Photographs showing the infrastructure and locations of the radomes of (a) the Doppler radar and (b) the dual-polarization radar on board the *Mirai*. Arrows with numbers nearby indicate ship facilities potentially blocking radar beams. The facilities are 1: marine-radar mast, 2-3: masts for restricted maneuvering light, 4: aft mast, 5: funnel, and 6: satellite downlink antenna.

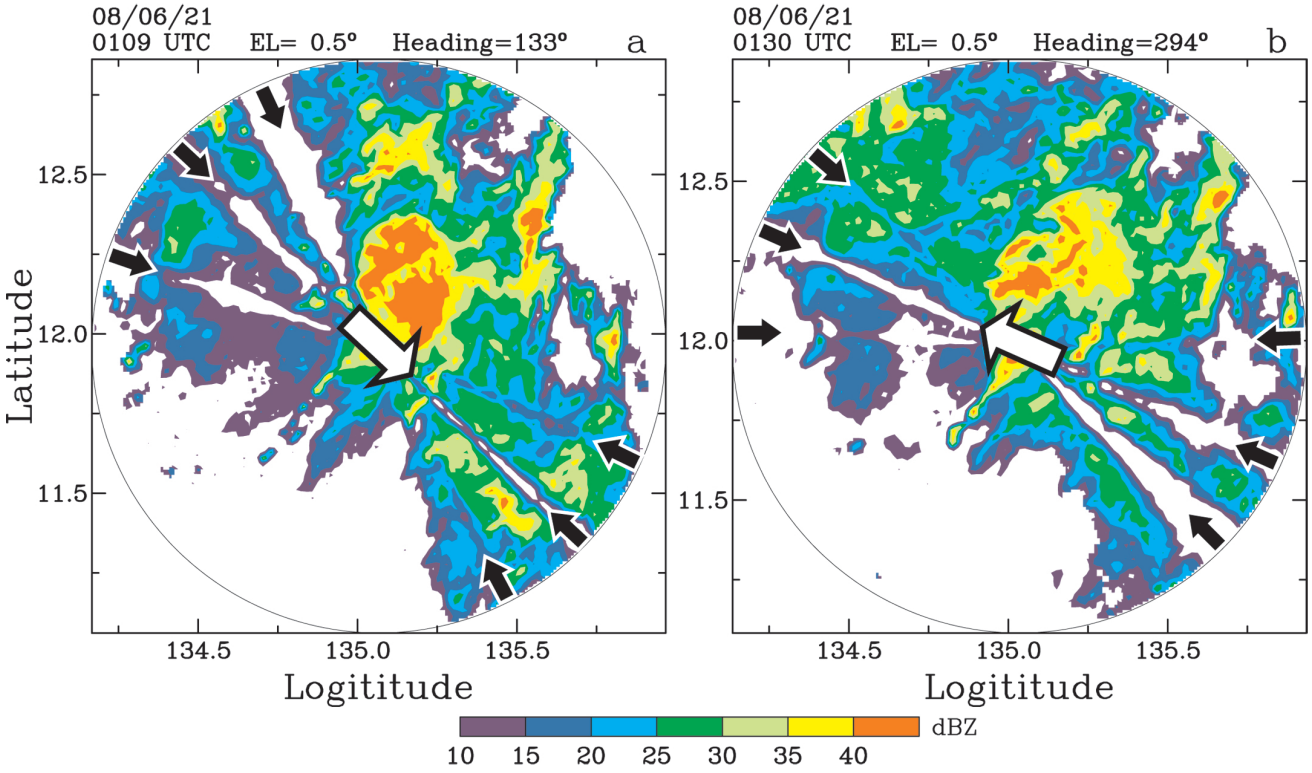

Fig. 2. Reflectivity at an elevation of 0.5 degrees observed by the Doppler radar at (a) 0109 UTC and (b) 0130 UTC 21 June 2008. Filled arrows outline the sectors where radar beams were affected by the ship's infrastructure. The open arrow at the center of each figure indicates the heading direction of the *Mirai*.

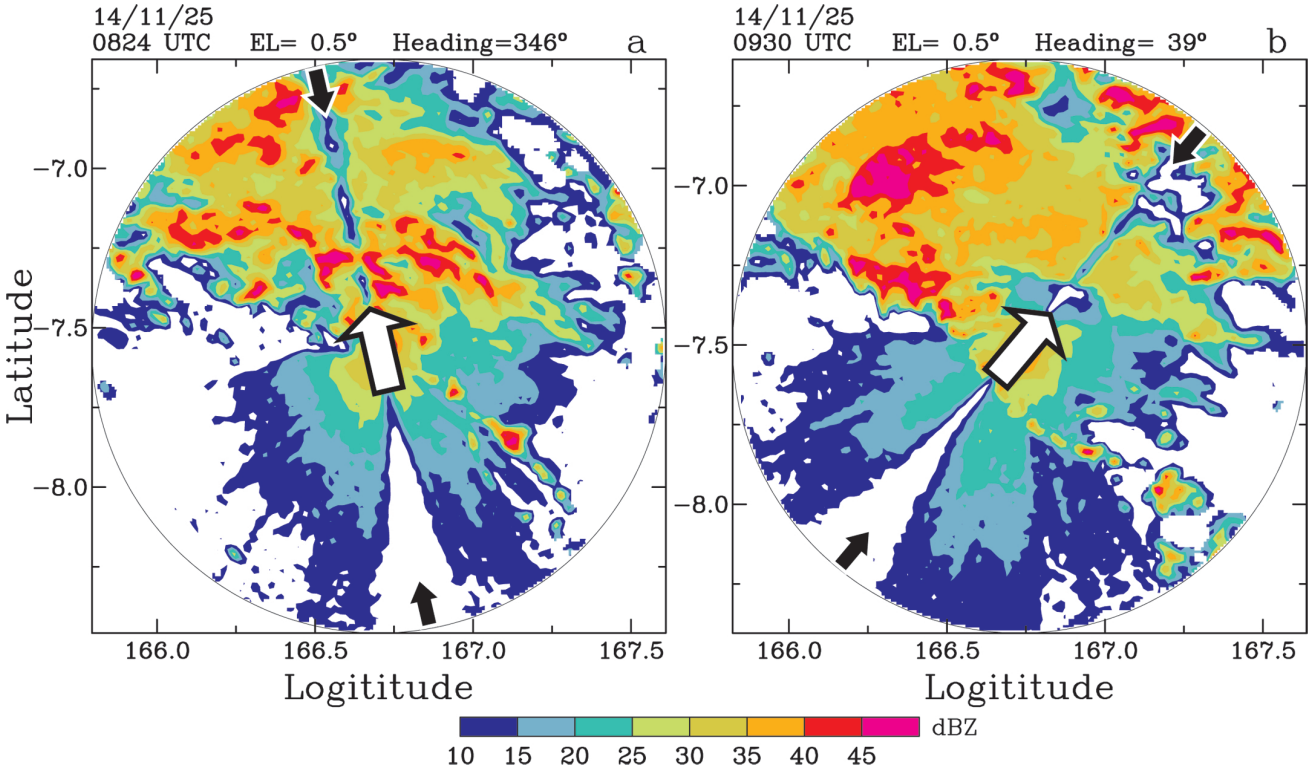

Fig. 3. As in Fig. 2, but for the reflectivity observed by the dual-polarization radar at (a) 0824 UTC and (b) 0930 UTC 25 November 2014.

3. Beam blockage identification

As shown in the previous section, radar beams were significantly blocked near the antennas of the Doppler and dual-polarization radars on board the *Mirai*. This section describes how to use archived reflectivity data to identify the location and size of the sectors suffering from beam blockage for both radars.

3.1 Dataset description

The information for the reflectivity data used in this study is shown in Table 2. These data are volume scans collected by the *Mirai* radars over the tropical Pacific and Indian oceans. Data from the cruises coded with MR08-02 (Yoneyama, 2008b) and MR11-07 (Yoneyama and Katsumata, 2011) were used for the Doppler radar. Over 13,500 volume scans are available, and each volume scan is composed of 21 ground-relative elevations. The data for the dual-polarization radar originate from cruises coded with MR14-06 Leg1 (Suetsugu, 2014) and MR14-06 Leg2 (Ando and Ueki, 2014). The dual-polarization radar performs an 18-elevation-step volume scan with 16,033 available volume scans. It should be noted that in order to obtain the data in a designated ground-relative elevation, the antennas of the *Mirai* radars are operated by compensating the attitude angles (heading, pitch, and roll) of the ship.

Radar parameters were calibrated at the beginning and end of each cruise listed above. The radar parameters were also checked every day during the observations. These regular maintenance activities enabled the *Mirai* radars to obtain stable and accurate data during the cruises.

3.2 Ship-relative POD maps

3.2.1 Definition

To assess beam blockage due to the infrastructure of the *Mirai*, the above archived reflectivity data were used to calculate the horizontal distribution of the probability of detection (POD). The POD is defined as the ratio of the number of reflectivity exceeding a certain threshold to the total number of observations taken at a given location. The POD is two dimensional and was calculated on a grid-by-grid basis in radar polar coordinates. In this study, a threshold of 10 dBZ was selected to calculate the POD.

The POD is given as a percentage, and the POD values range from 0 to 100. If no echo is detected, the value of the POD will be 0, and if an echo is always observed, the value of the POD will be 100. These features facilitate the identification of radar beam blockage. Through calculating the POD over a long period when sufficient precipitation occurred, beam blockage can easily be detected and identified. As seen from Figs. 2 and 3, radar echoes were missing or significantly deficient in the sectors where radar beams were completely or partially blocked. This indicates that the POD values in sectors suffering from beam blockage should be lower than those in surrounding sectors that are not blocked. Furthermore, the interfaces between the blocked and unblocked sectors should be bounded by a tight POD gradient.

The POD method has been widely used to identify beam blockage for ground radars that are surrounded by obstacles such as mountains and buildings (Sugier et al., 2002; Kucera et al., 2004; Krajewski et al., 2006; Chang et al., 2009; Lakshmanan et al., 2012). Maps of the POD are often made for different antenna elevations. The POD for ground radars is calculated at a ground-relative azimuth and elevation.

However, the *Mirai* radars are mobile. The antennas of the *Mirai* radars are operated by compensating the movement and inclination of the ship. It is clear from Figs. 2 and 3 that ground-relative directions of the blocked sectors

Table 2. Archived reflectivity data used in the paper.

	Doppler radar	Dual-polarization radar
Cruise Codes	MR08-02, MR11-07	MR14-06
Periods of data	May 29~Jun. 29, 2008, Sep. 25~Oct. 26, 2011, Oct. 29~Dec. 01, 2011	Nov. 7~Dec.18, 2014, Dec. 20, 2014~ Jan. 17, 2015
Ground-relative elevations of a volume scan (degree)	0.5, 1.0, 1.8, 2.6, 3.4, 4.2, 5.0, 5.8, 6.7, 7.7, 8.9, 10.3, 12.3, 14.5, 17.1, 20.0, 23.3, 27.0, 31.0, 35.4, 40.0	0.5, 1.0, 1.7, 2.4, 3.1, 3.8, 4.6, 5.6, 6.7, 8.2, 10.3, 12.8, 15.8, 19.4, 23.6, 28.4, 33.7, 40.0
Volume-scan intervals (minute)	10	6
Number of volume scans	13,513	16,033

for the *Mirai* radars vary with the movement of the ship. Therefore, in order to assess beam blockage caused by the infrastructure of the *Mirai*, the POD for the *Mirai* radars should be calculated at a ship-relative azimuth and elevation.

In this study, the ship-relative azimuth was defined as the horizontal angle from the bow of the *Mirai*. The relative azimuth plus the heading of the *Mirai* combine to provide the true (ground-relative) azimuth. In addition, the ship-relative elevation was defined as the angle of the antenna in a vertical direction above the deck of the *Mirai*. Zero and 90 degrees indicate the directions parallel and normal to the deck of the *Mirai*, respectively. The ship-relative elevations used to calculate the POD are shown in Table 3. The ship-relative elevations were selected based on the ground-relative elevations of the volume scans listed in Table 2. The selection was made to ensure that there were sufficient data to calculate the POD at each specific ship-relative elevation.

3.2.2 POD maps and beam blockage patterns

An example of the POD maps for the Doppler and dual-polarization radars at a ship-relative elevation of 0.5 degrees is shown in Fig. 4. Note that the azimuth in Fig. 4 is relative to the *Mirai*. As a result, the 'north' and 'south' in Fig. 4 are toward the bow and stern of the *Mirai*, respectively. There are two notable features in the POD field related to beam blockage for both radars.

The first is associated with values of the POD.

Table 3. Ship-relative elevations for identifying radar beam blockage.

	Doppler radar	Dual-polarization radar
Ship-relative elevations (degree)	0.0, 0.5, 1.0, 1.5, 2.0, 2.5, 3.0, 3.5, 4.0, 4.5, 5.0, 5.5, 6.0, 6.5, 7.0, 7.5, 8.0, 8.5, 9.0, 9.5, 10.5, 11.5, 12.5, 13.5, 14.5, 15.5, 17.0, 18.5, 20.0, 23.5, 27.0, 31.0, 35.5, 40.0	0.0, 0.5, 1.0, 1.5, 2.0, 2.5, 3.0, 3.5, 4.0, 4.5, 5.0, 5.5, 6.0, 7.0, 8.0, 9.0, 10.0, 11.5, 13.0, 14.5, 16.0, 19.5, 23.5, 28.5, 33.5, 40.0

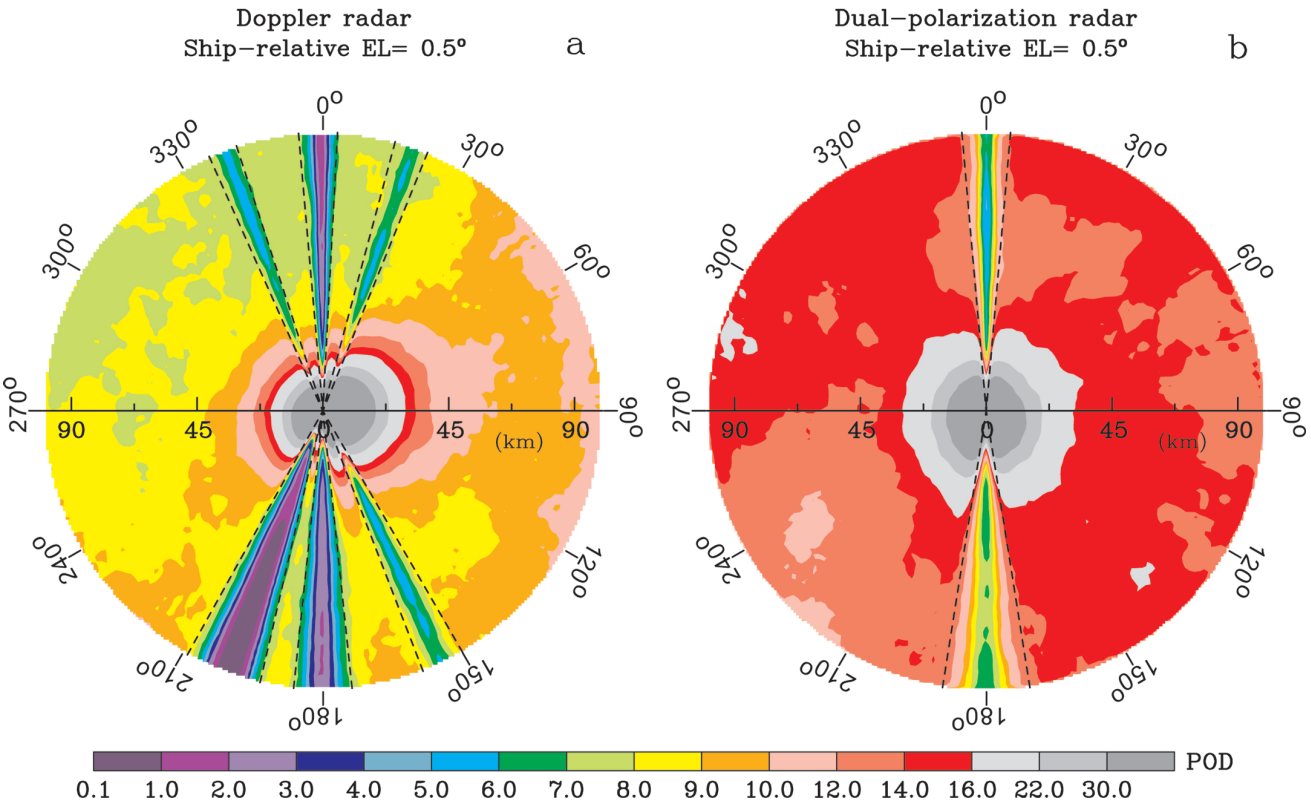

Fig. 4. POD maps at a ship-relative elevation of 0.5 degrees for (a) the Doppler radar and (b) the dual-polarization radar. The azimuth of the figure is relative to the *Mirai*, which is the horizontal angle from the bow of the ship. Dashed lines outline the blocked sectors identified by using the method described in section 3.3.

There were several azimuthal sectors with local minimum values of the POD. For the Doppler radar (Fig. 4a), six such sectors were found around ship-relative azimuths of 340, 0, 19, 155, 180, and 201 degrees. The POD values in these sectors were significantly lower than those in their surroundings. These minimum POD sectors were in good agreement with the sectors where radar echoes were missing or significantly deficient (Fig. 2). As shown in Fig. 1, there were corresponding facilities in the directions of these minimum POD sectors. The minimum POD sectors on the bow side of the radar were related to the marine-radar mast and the masts for the restricted maneuvering light, respectively. The minimum POD sectors on the stern side of the radar were associated with the aft mast, funnel, and satellite downlink antenna, respectively.

As for the dual-polarization radar (Fig. 4b), there were two sectors with local minimum POD values near the ship-relative azimuths of 0 and 180 degrees. These minimum POD sectors also corresponded well to the sectors with missing or significantly deficit echoes from the radar (Fig. 3) and were in the directions of the marine-radar mast and aft mast, respectively (Fig. 1). It is obvious that the azimuthal sectors with the local POD minima as seen in Fig. 4 were blocked sectors that appeared as a result of the blocking of radar beams by the infrastructure of the *Mirai*.

The other notable feature in the POD field is related to the azimuthal gradient of the POD. Relatively high values of the POD were found in regions outside the blocked sectors described above (Fig. 4), suggesting that these regions were unblocked. Interfaces between the unblocked and blocked sectors were characterized by abrupt transition zones where the POD dropped significantly toward the blocked sectors. Significant azimuthal discontinuities in the POD field were observed on the edges of the blocked sectors, resulting in strong azimuthal POD gradients. It should be noted that the POD in the unblocked sectors also varied in the azimuthal direction, which can be attributed to the nonhomogeneous precipitation distribution. Nevertheless, the azimuthal change of the POD in the unblocked sectors was relatively slight, which resulted in a weak POD gradient.

It should be noted in Fig. 4 that the POD was much higher within the first 30 km of both radars. This was the result of sea clutter echoes. Nevertheless, the significantly decreased POD in the blocked sectors was evident far away from the radars and consistent in the radial direction. This indicates that the contamination of sea clutter has little influence on the use of the POD to discriminate beam blockage due to the infrastructure of the *Mirai*.

Although the calculated POD maps illustrate the patterns of beam blockage very well, the boundaries of the blocked sectors needed to be ascertained. It appears that the distinct azimuthal variation of the POD around the blocked sectors could facilitate the ascertainment of their boundaries.

3.3 Boundaries of blocked sectors

In this study, the azimuthal boundaries of a sector suffering from partial or total beam blockage were defined as places where the POD begins to fall significantly in the azimuthal direction. In order to objectively ascertain the boundaries of a blocked sector, the rate of change of the POD gradient (RCPG) along the azimuthal direction must be calculated. The mathematical definition of the RCPG is

$$\mathrm{RCPG}\,(i, j) = \frac{\partial}{\partial_j}\left|\frac{\partial POD\,(i, j)}{\partial_j}\right| \quad , \qquad (1)$$

where the indices i and j represent the ranges and azimuths, respectively. The ascertainment of the boundaries of a blocked sector through the RCPG is simple and straightforward because the maximum and minimum of the RCPG represent the beginning and end of a significant change in the POD, respectively.

It can be seen from Figs. 2, 3, and 4 that the patterns of beam blockage due to the infrastructure of the *Mirai* are consistent in the radial direction. As a result, both the POD and RCPG were averaged in the radial direction and their mean values were utilized for the discrimination of the boundaries of the blocked sectors. To reduce the effect of sea clutter, data in a horizontal range close to the radars were not used in computing the average. The horizontal range affected by sea clutter was set to vary with elevation, 30 km and 5 km in the lowest and highest elevations, respectively.

An example of the azimuthal variation of the mean POD and RCPG values for the dual-polarization radar at a ship-relative elevation of 0.5 degrees is shown in Fig. 5a. Five passes of a 1-2-1 filter were applied to the mean POD and RCPG to eliminate small fluctuations. The notable features of beam blockage in the POD field as described in section 3.2.2 are readily apparent in the plot. Two blocked sectors seen in Fig. 4b are reflected in Fig. 5a by two prominent minima of the mean POD near ship-relative azimuths of 0 and 180 degrees, respectively. Toward each of the minima, the mean POD dropped significantly from both

sides. Consistently with the distinct variation of the mean POD, the mean RCPG also changed substantially.

The azimuthal variation of the mean POD and RCPG around one of the blocked sectors in Fig. 5a is enlarged in Fig. 5b; this will be used to explain the ascertainment of the boundaries of a blocked sector. The minimum of the mean POD caused by beam blockage is marked by P_{min}. It is evident that a few of the maximum and minimum of the mean RCPG exist on both sides of the P_{min}. To the left (decreasing azimuth side) of the P_{min}, the maximum of the mean RCPG (LR_{max}) indicates the beginning of a sharp fall of the mean POD from the left of the P_{min}. To the right (increasing azimuth side) of the P_{min}, the minimum of the mean RCPG (RR_{min}) indicates the end of a sharp rise of the mean POD toward the right of the P_{min}, or in other words, the beginning of a sharp fall of the mean POD from the right of the P_{min}. The minimum and maximum of the mean RCPG immediately on the left and right sides of the P_{min} represent the end of the sharp fall and the beginning of the sharp rise on each side, respectively. It is evident that the signatures of the LR_{max} and RR_{min} are purely deterministic. Consequently, by finding the maximum RCPG on the left side and the minimum RCPG on the right side of the minimum POD associated with a blocked sector, the boundaries of the blocked sector, defined as the places where the POD begins to fall significantly due to partial or total beam blockage, can be easily ascertained.

It is worth mentioning that the effect of partial beam blockage outside the ascertained boundaries could not be directly examined in this study. Nevertheless, after plotting

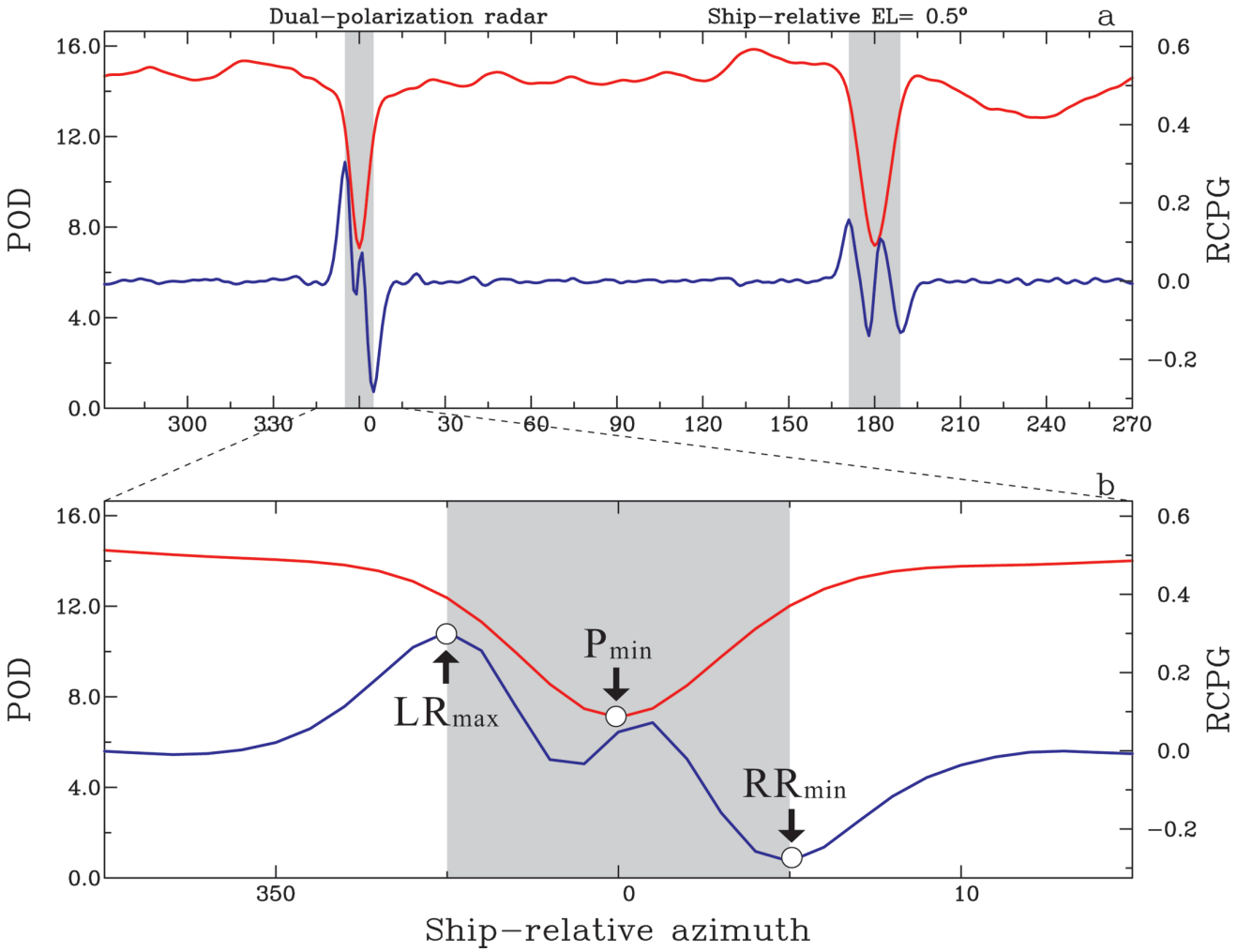

Fig. 5. (a) Azimuthal trend of the mean POD (red curve) and mean RCPG (blue curve) at a ship-relative elevation of 0.5 degrees for the dual-polarization radar. All curves were smoothed with five passes of a 1-2-1 filter. Grey shaded regions represent the identified blocked sectors. (b) As in (a), but in a much smaller azimuthal range of (a). Three circles indicate the important points used to assess the size of a blocked sector, which are described in detail in section 3.3.

the boundaries of the blocked sectors assessed by using the above method on the POD maps (see Fig. 4, for example), we found that the POD immediately outside the ascertained boundaries of the blocked sectors was in harmony with the high POD in the unblocked sectors. This result suggests that the effect of partial beam blockage would be less important outside the ascertained boundaries. It appears that the boundaries of the blocked sectors determined by using the maximum and minimum of the RCPG would have enclosed significantly decreased values of the POD caused by partial beam blockage.

In summary, the identification of beam blockage caused by the infrastructure of the *Mirai* includes five steps:

1. Make POD maps at a ship-relative azimuth and elevation.

2. Find azimuthal sectors with pronounced minima of the POD in their centers and significant discontinuities of the POD on their edges. These sectors represent the blocked sectors.

3. Compute the RCPG using equation (1).

4. Compute mean POD and RCPG by averaging them in the radial direction.

5. Find the maximum and minimum of the mean RCPG on the left and right sides, respectively, of the minimum of the mean POD associated with each blocked sector. The locations of the maximum and minimum of the mean RCPG represent the boundaries of the blocked sector.

4. Characteristics of beam blockage for the *Mirai* radars

The method described in the previous section facilitates a quantitative investigation of beam blockage for the *Mirai* radars. The number and azimuthal range of blocked sectors in different ship-relative elevations were ascertained and are shown in Table 4 for the Doppler radar and Table 5 for the dual-polarization radar.

As for the Doppler radar, there were six blocked sectors below a ship-relative elevation of 3 degrees. The number of blocked sectors then decreased with increasing elevation, becoming two between elevations of 6.5 and 20 degrees and one at higher elevations. As for the dual-polarization radar, there were only two blocked sectors below a ship-relative elevation of 16 degrees, and one blocked sector at higher elevations. The decrease in the number of the blocked sectors could be attributed

Table 4. Sectors affected by beam blockage for the Doppler radar.

Ship-relative elevations (degree)	Number of sectors	Ship-relative azimuths (degree)	Ship-relative elevations (degree)	Number of sectors	Ship-relative azimuths (degree)
0.0	6	336~343, 355~3, 15~22, 150~160, 174~186, 192~209	0.5	6	336~342, 355~3, 15~22, 150~159, 174~186, 193~209
1.0	6	336~342, 355~3, 15~22, 150~159, 173~186, 193~208	1.5	6	336~342, 355~3, 15~22, 150~159, 173~187, 193~208
2.0	6	336~342, 355~3, 15~22, 150~159, 174~187, 193~208	2.5	6	336~342, 355~4, 15~22, 150~159, 174~187, 193~207
3.0	6	336~342, 355~4, 15~22, 150~159, 173~187, 193~207	3.5	5	336~342, 355~4, 15~22, 173~187, 193~207
4.0	5	335~342, 355~4, 15~22, 172~188, 193~207	4.5	5	335~342, 355~4, 15~22, 173~188, 193~207
5.0	5	335~342, 355~4, 15~22, 172~188, 193~207	5.5	4	335~342, 354~4, 15~22, 172~188
6.0	3	354~4, 15~22, 171~188	6.5	2	354~4, 171~188
7.0	2	354~4, 171~188	7.5	2	354~4, 170~188
8.0	2	354~4, 171~188	8.5	2	354~4, 170~188
9.0	2	354~4, 170~188	9.5	2	354~4, 170~188
10.5	2	354~4, 170~188	11.5	2	354~4, 170~188
12.5	2	354~4, 170~188	13.5	2	354~4, 170~188
14.5	2	354~4, 167~188	15.5	2	354~5, 167~188
17.0	2	354~5, 168~188	18.5	2	354~5, 168~188
20.0	2	354~5, 170~188	23.5	1	168~188
27.0	1	168~187	31.0	1	170~187
35.5	1	171~187	40.0	1	171~187

to the increased height of the radar antenna for the dual-polarization radar (Table 1). For both radars, the blocked sectors near ship-relative azimuths of 0 and 180 degrees, respectively, existed from low to high ship-relative elevations. It appears that the marine-radar mast and aft mast, as seen in Fig. 1, have a substantial effect on beam blockage for the *Mirai* radars.

Table 5. Sectors affected by beam blockage for the dual-polarization radar.

Ship-relative elevations (degree)	Number of sectors	Ship-relative azimuths (degree)	Ship-relative elevations (degree)	Number of sectors	Ship-relative azimuths (degree)
0.0	2	355~5, 171~190	0.5	2	355~5, 171~189
1.0	2	355~5, 171~189	1.5	2	355~5, 171~189
2.0	2	355~5, 171~189	2.5	2	355~5, 171~189
3.0	2	355~5, 171~189	3.5	2	355~5, 171~189
4.0	2	355~5, 172~188	4.5	2	355~5, 172~189
5.0	2	355~6, 172~189	5.5	2	354~6, 172~189
6.0	2	354~6, 171~189	7.0	2	355~6, 171~189
8.0	2	355~7, 172~189	9.0	2	355~6, 172~189
10.0	2	355~6, 171~188	11.5	2	355~7, 172~189
13.0	2	355~7, 171~188	14.5	2	355~7, 172~189
16.0	2	356~7, 171~188	19.5	1	172~189
23.5	1	172~189	28.5	1	171~189
33.5	1	171~188	40.0	1	172~188

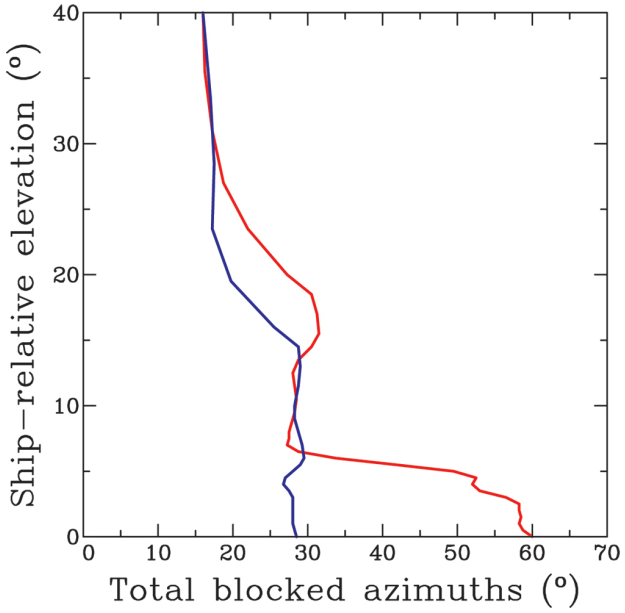

Fig. 6. Variation of total azimuths affected by beam blockage with ship-relative elevation for the Doppler radar (red curve) and dual-polarization radar (blue curve).

The trend of total blocked azimuths with ship-relative elevation is plotted in Fig. 6. Accompanying the reduction in the number of the blocked sectors, the total blocked azimuths for both radars decreased with increasing elevation. It was evident that significantly more improvement of beam blockage by the dual-polarization radar was achieved below a ship-relative elevation of 2.5 degrees. At this low elevation level, the total blocked azimuths for the Doppler radar was near 60 degrees. In contrast, the total blocked azimuths for the dual-polarization radar was less than 30 degrees. It was evident that the total azimuths of the low-level blocked sectors for the dual-polarization radar decreased by more than half, which in turn considerably increased the coverage of the dual-polarization radar. The increase in the radar convergence at low elevations is very significant for rainfall estimation, because low-elevation radar data provide the most useful and reliable information for rainfall rates (Joss and Waldvogel, 1990). Consequently, confident rainfall estimation has improved significantly with dual-polarization radar.

5. Some potential applications

Beam blockage for the Doppler and dual-polarization radars on board the *Mirai* was ascertained in detail for the first time. An obvious application of this study concerns the quality control of the *Mirai* radar data. The accurate beam blockage information derived from this study facilitated the correction and removal of echoes and polarimetric parameters at locations where radar beams were blocked by the infrastructure of the *Mirai*. This type of data processing is imperative for improving quantitative precipitation estimation (QPE). It appears that the results of this study will improve QPE using the data observed by the *Mirai* radars.

In this study, the information of beam blockage at different ship-relative elevations was ascertained for the *Mirai* radars by using archived reflectivity data. This information was dependent on ground-relative elevations of volume scans of the archived data. For radar observations

with volume-scan elevations different from those in this study, new information on beam blockage would be necessary for the quality control of the *Mirai* radar data. The beam blockage algorithm developed in this study is based only on archived reflectivity data and purely deterministic signatures of the POD, which can be easily used to assess beam blockage for various data observed by the *Mirai* radars in a similar way as shown in section 3.

6. Summary and conclusions

A Doppler weather radar has been in service on board the research vessel *Mirai* since 1998. The Doppler radar was replaced by a dual-polarization Doppler weather radar in 2014. Radar beams from both radars were blocked by the infrastructure of the *Mirai* in several directions, where radar echoes were missing or significantly deficient from the radars.

The beam blockage for each of the *Mirai* radars was investigated in this study. The ascertainment of beam blockage was based on a statistical analysis of reflectivity data from long-term observations. Data of more than 10,000 volume scans from each of the radars were used to calculate the distribution of the probability of detection (POD), which is the ratio of the number of reflectivities greater than 10 dBZ to the total number of observations taken at a given range, azimuth, and elevation relative to the *Mirai*.

The calculated POD field revealed distinct signatures related to beam blockage for both radars. There exist several azimuthal sectors where the POD was significantly lower than the surroundings, forming distinct local minima of the POD. Corresponding infrastructure of the *Mirai* was found in the directions of the minimum POD sectors, indicating that these minimum POD sectors were blocked sectors caused by the infrastructure of the *Mirai*. In addition, significant azimuthal discontinuities of the POD existed on the edges of the blocked sectors.

The azimuthal boundary on either side of a blocked sector was defined as the place where the POD begins to fall significantly in the azimuthal direction. An objective method was developed to ascertain the boundaries of the blocked sectors found from the horizontal distribution of the POD. The method is based on the rate of change of the POD gradient (RCPG) along the azimuthal direction. It utilizes a purely deterministic maximum and minimum RCPG on the left and right edges of a blocked sector, respectively. The ascertained boundaries enclose the discontinuous regions of the POD caused by beam blockage and clearly distinguish the blocked sectors from the unblocked sectors.

Digital beam blockage information for both radars was identified at different ship-relative elevations. It was found that radar beams from both radars were blocked from low to high elevations. At low elevations, however, the degree of beam blockage was significantly improved by the dual-polarization radar, primarily because of the increase in antenna height. As a result, the low-level coverage of the dual-polarization radar became much greater than that of the Doppler radar.

The accurate beam blockage information provided in this study will facilitate the quality control of the *Mirai* radar data. The simple and straightforward method used to ascertain beam blockage can be easily applied to various data observed by the *Mirai* radars.

Acknowledgements

The authors would like to express their deep appreciation to the entire crew of the research vessel *Mirai* and to the technical staffs of Global Ocean Development Inc. for their support in conducting radar observations and data archiving.

References

Ando, K., and I. Ueki (2014), R/V MIRAI Cruise Report MR14-06 Leg2 and Leg3, *JAMSTEC MIRAI Cruise Reports*, <http://www.godac.jamstec.go.jp/catalog/data/doc_catalog/media/MR14-06_leg2_all.pdf>.

Bech, J., B. Codina, J. Lorente, and D. Bebbington (2003), The sensitivity of single polarization weather radar beam blockage correction to variability in the vertical refractivity gradient, *J. Atmos. Oceanic Technol.*, *20*, 845-855.

Bech, J., U. Gjertsen, and G. Haase (2007), Modelling weather radar beam propagation and topographical blockage at northern high latitudes, *Q. J. R. Meteorol. Soc.*, *133*, 1191-1204.

Chang, P.-L., P.-F. Lin, B. J.-D. Jou, and J. Zhang (2009), An application of reflectivity climatology in constructing radar hybrid scans over complex terrain, *J. Atmos.*

Oceanic Technol., 26, 1315-1327.

Geng, B., K. Yoneyama, R. Shirooka, and M. Yoshizaki (2011), Characteristics of precipitation systems and their environment observed during the onset of the western North Pacific summer monsoon in 2008, *J. Meteor. Soc. Japan*, *89A*, 1-25.

Giangrande, S. E., and A. V. Ryzhkov (2005), Calibration of dual-polarization radar in the presence of partial beam blockage, *J. Atmos. Oceanic Technol.*, *22*, 1156-1166.

Inoue, J., M.E. Hori, Y. Tachibana, and T. Kikuchi (2010), A polar low embedded in a blocking high over the Pacific Arctic, *Geophys. Res. Lett.*, *37*, L14808, doi:10.1029/2010GL043946.

Joss, J., and A. Waldvogel (1990), Precipitation measurement and hydrology, In: Radar in Meteorology, D. Atlas (Ed.), AMS, 577-606.

Katsumata, M., and K. Yoneyama (2004), Internal structure of ITCZ mesoscale convective systems and related environmental factors in the western Pacific: An observational case study, *J. Meteor. Soc. Japan*, *82*, 1035-1056.

Katsumata, M., T. Ushiyama, K. Yoneyama, and Y. Fujiyoshi (2008), Combined use of TRMM/PR and disdrometer data to correct reflectivity of ground-based radars, *SOLA*, *4*, 101-104.

Katsumata, M. (2014), On the new shipboard Doppler radar of the R/V Mirai, *Tenki*, *61*, 871-875 (in Japanese).

Krajewski, W. F., A. Ntelekos, and R. Goska (2006), A GIS based methodology for the assessment of weather radar beam blockage in mountainous regions: Two examples from the U.S. NEXRAD network, *Comput. Geosci.*, *32*, 283-302.

Kucera, P. A., W. F. Krajewski, and C. B. Young (2004), Radar beam occultation studies using GIS and DEM technology: An example study of Guam, *J. Atmos. Oceanic Technol.*, *21*, 995-1006.

Lakshmanan, V., J. Zhang, K. Hondl, and C. Langston (2012), A statistical approach to mitigating persistent clutter in radar reflectivity data, *IEEE J. Sel. Top. Appl. Earth Obs. Remote Sens.*, *5*, 652-662.

Lang, T. J., S. W. Nesbitt, and L. D. Carey (2009), On the correction of partial beam blockage in polarimetric radar data, *J. Atmos. Oceanic Technol.*, *26*, 943-957.

Shakti, P. C., M. Maki, S. Shimizu, T. Maesaka, D.-S. Kim, D.-I. Lee, and H. Iida (2013), Correction of Reflectivity in the Presence of Partial Beam Blockage over a Mountainous Region Using X-Band Dual Polarization Radar, *J. Hydrometeor*, *14*, 744-764.

Suetsugu, D. (2014), MIRAI MR14-06 Leg1 Cruise Report, *JAMSTEC MIRAI Cruise Reports*, 85 pp., <http://www.godac.jamstec.go.jp/catalog/data/doc_catalog/media/MR14-06_leg1_all.pdf>.

Sugier, J., J. Parent du Chatelet, P. Roquain, and A. Smith (2002), Detection and removal of clutter and anaprop in radar data using a statistical scheme based on echo fluctuation, In: Proc. ERAD, EMS, Copernicus GmbH, 17-24.

Villarini, G., and W. F. Krajewski (2010), Review of the different sources of uncertainty in single polarization radar-based estimates of rainfall, *Surv. Geophys.*, *31*, 107-129.

Vivekanandan, J., D. N. Yates, and E. A. Brandes (1999), The influence of terrain on rainfall estimates from radar reflectivity and specific propagation phase observations, *J. Atmos. Oceanic Technol.*, *16*, 837-845.

Westrick, K. J., C. F. Mass, and B. A. Colle (1999), The limitations of the WSR-88D radar network for quantitative precipitation measurement over the coastal western United States, *Bull. Amer. Meteor. Soc.*, *80*, 2289-2298.

Yamada, H., K. Yoneyama, M. Katsumata, and R. Shirooka (2010), Observations of a super cloud cluster accompanied by synoptic-scale eastward-propagating precipitating systems over the Indian Ocean, *J. Atmos. Sci.*, *67*, 1456-1473.

Yoneyama, K. (1998), On the shipboard Doppler radar of the R/V Mirai, *Tenki*, *45*, 133-136 (in Japanese).

Yoneyama, K., and Coauthors (2008a), MISMO field experiment in the equatorial Indian Ocean, *Bull. Amer. Meteor. Soc.*, *89*, 1889-1903.

Yoneyama, K. (2008b), R/V MIRAI Cruise Report MR08-02, *JAMSTEC MIRAI Cruise Reports*, 86 pp., <http://www.godac.jamstec.go.jp/catalog/data/doc_catalog/media/MR08-02_all.pdf>.

Yoneyama, K., and M. Katsumata (2011), R/V MIRAI Cruise Report MR11-07, *JAMSTEC MIRAI Cruise Reports*, 350 pp., <http://www.godac.jamstec.go.jp/catalog/data/doc_catalog/media/MR11-07_leg1-2_all.pdf>.

Yoneyama, K., C. Zhang, and C. N. Long (2013), Tracking pulses of the Madden-Julian oscillation, *Bull. Amer. Meteor. Soc.*, *94*, 1871-1891.

Young, C. B., B. R. Nelson, A. A. Bradley, J. A. Smith, C. D. Peters-Lidard, A. Kruger, and M. L. Baeck (1999), An evaluation of NEXRAD precipitation estimates in complex terrain, *J. Geophys. Res.*, *104*, 19691-19703.